

Vorticity transport associated with the dominant vortical structure of twin jets in crossflow

V.Kolář¹, H.Takao², T.Todoroki², E.Savory³, S.Okamoto² and N.Toy³

¹Institute of Hydrodynamics, Academy of Sciences of the Czech Rep.
166 12 Prague 6, CZECH REPUBLIC

²Department of Mechanical Engineering, Shibaura Institute of Technology
Shibaura 3-9-14, Minato-ku, Tokyo 108, JAPAN

³Fluids Research Centre, School of Engineering
University of Surrey, Guildford GU2 7XH, U.K.

Abstract

The present work is concerned with “twin jets in crossflow” (TJICF), where the configuration consists of a pair of identical jet nozzles and jet-flow conditions at the nozzle exits. The mean flow velocity vector and associated turbulence statistics of the TJICF have been determined using the standard crossed hot-wire anemometry technique. In the present contribution two geometrically symmetric TJICF arrangements, namely tandem and side-by-side arrangements (both with a nozzle centre-to-centre separation of 5D), are examined, focusing upon the dominant vortical structure rather similar to that of the well-known contrarotating vortex pair (CVP) of the single JICF. The formation and decay of this dominant vortical structure is closely associated with the turbulent vorticity transport. The two TJICF arrangements under consideration have their own specific vorticity features which are, firstly, visualized and interpreted in terms of turbulent vorticity fluxes. Secondly, the vorticity transport analysis shows the vortex-strength decay (i.e. circulation decay) as described by the corresponding integral decay-rate formula. The similarities and differences between the vorticity features associated with the two different TJICF (i.e. tandem and side-by-side) arrangements and the single jet case are examined and discussed. The TJICF flow phenomenon represents an interaction of two single JICFs and the gross qualitative features of the vortex formation process of resulting (mean-flow) dominant vortical structure are described.

Introduction

Many engineering and environmental problems deal with the basic jet-flow configuration of a single circular jet issuing normally into a crossflow (JICF) that has already been investigated by researchers for more than fifty years (cf. Margason [12]). The typical engineering applications include the aerodynamics of ASTOVL aircraft and jet steering systems, combustion chamber mixing, environmental flows such as vehicle exhaust and chimney plume dispersion etc.

The practical applications may need, for a variety of reasons like efficiency, a substitution of the single JICF by multiple jets in crossflow. The present contribution deals with “twin jets in crossflow” (referred to as TJICF), where the configuration consists of a pair of identical jet nozzles and jet-flow conditions at the nozzle exits. Two geometrically symmetric TJICF arrangements, namely tandem and side-by-side arrangements, with a nozzle centre-to-centre separation of approx. 5D, were chosen for an experimental study concentrating upon the vorticity distribution and turbulent vorticity transport associated with the dominant vortical structure found rather similar to that of the well-known contrarotating vortex pair (CVP) of the single JICF.

While hundreds of papers have studied the single JICF problem in detail, the literature on the TJICF problem is relatively scarce,

e.g. Holdemann and Walker [5], Makihata and Miyai [11], Gregoric, Davis and Bushnell [4], Isaac and Jakubowski [6], Karagozian, Nguyen and Kim [7], Savory and Toy [15], Barata, Durão, Heitor and McGuirk [1]. These papers bring useful information predominantly on global characteristics such as jet path or vortex trajectory, on multiple or confined multiple jets in crossflow by varying number of jets in a row, or considering specific geometrical configurations of nozzles (including their overlapping). The present authors are unaware of any TJICF study dealing with the vorticity distribution and vorticity transport within the dominant vortical structure, namely the resulting CVP. For the single JICF the CVP occurs as a result of the impulse of the jet on the crossflow, forming itself in the near field and becoming dominant in the far field—for a description of the fundamental vortical structure associated with the JICF flow phenomenon see Fric and Roshko [3], Morton and Ibbetson [13].

The formation and decay of the dominant vortical structure of the TJICF, approaching downstream—according to the present results—the single CVP structure both for the tandem and side-by-side arrangements, is closely associated with the turbulent vorticity transport. However, the two TJICF arrangements under consideration have their own specific vorticity distributions and, especially, distinct vorticity transport features which are visualized and interpreted in terms of turbulent vorticity fluxes (for definition see Kolář, Lyn and Rodi [8]). The vorticity transport analysis shows the vortex-strength decay (i.e. circulation decay) as described by the corresponding integral decay-rate formula (for 2D case derived and applied by Kolář [9]). The 3D vorticity transport analysis has been recently applied to the single JICF by Kolář, Savory and Toy [10].

Although the CVP has mean-flow definition it may have unsteady components as pointed out by Fric and Roshko [3]. So, it is well recognized that large-scale organized vortical structures may exist within the flow field, such as the double-helical morphology of the JICF coherent structure revealed recently by Papaspyros, Kastrinakis and Nychas [14]. In the present work these unsteady components of the fluid motion are not taken into account and are reflected as an inherent contribution to the *long-time-averaged* values of relevant quantities (denoted below by angular brackets $\langle \dots \rangle$).

Experimental Details

The measurements were carried out in a wind tunnel in the Department of Civil Engineering at the University of Surrey, using the standard crossed hot-wire anemometry technique. The tunnel working cross-section was 0.62 m width \times 0.75 m height and the twin jet nozzles of diameter $D = 13.5$ mm were placed flush with the ground plane. Both tandem and side-by-side arrangements were considered for a single case with a nozzle

centre-to-centre separation of approx. $5D$ (66.3 mm, i.e. $4.91D$). The jet outlet velocity was $U_J = 25.0$ m/s, resulting in $Re_J \approx 2.24 \times 10^4$. Only one jet-velocity/crossflow-velocity ratio, $R = U_J/U_C$, was studied, namely the ratio $R = 8$. Hence, the crossflow velocity was set to be $U_C = 3.125$ m/s. The flow symmetry is assumed in order to reduce the range of measurements to a half-plane. The coordinate system is shown for both geometrical configurations in figure 1(a, b) with the origin located at the centre in between the nozzles.

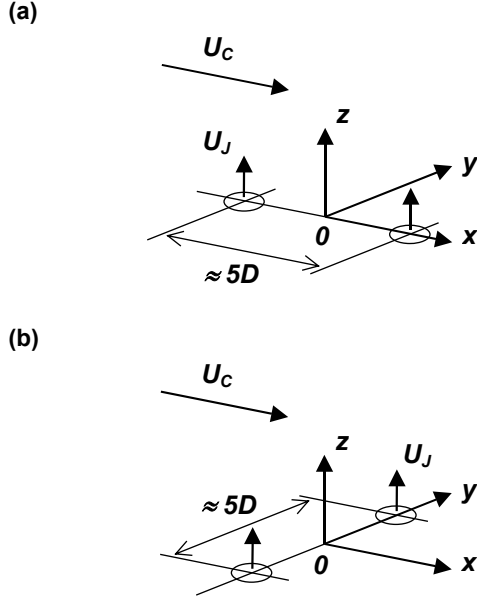


Figure 1. Coordinate system: (a) tandem, (b) side-by-side arrangement.

The crossed hot-wire measurements were, whenever necessary, undertaken with a tilted probe that was approximately aligned with the pre-estimated mean flow direction and the Reynolds stresses of interest were reconstructed based on the decompositions in the manner of Cutler and Bradshaw [2] using four probe roll positions. In the present case there is no wall effect and the probe volume is relatively small in comparison with the flow structures being investigated. Hence, the gradient errors will be within the bounds found previously [2].

The velocity fields, that is the projections of the velocity vectors, $(\langle u \rangle, \langle v \rangle, \langle w \rangle)$, in the planes $x = \text{Const.}$, were determined in five equidistant rectangular cross sections located at $x/D = 10, 12.5, 15, 17.5$ and 20 with (max.) dimensions for tandem arrangement $z = 40\text{--}310$ mm ($z/D \approx 3\text{--}23$), $y = 0\text{--}130$ mm ($y/D \approx 0\text{--}9.6$), and for side-by-side arrangement $z = 10\text{--}250$ mm ($z/D \approx 0.7\text{--}18.5$), $y = 0\text{--}150$ mm ($y/D \approx 0\text{--}11.1$) with a square measurement mesh having steps of 10 mm. Some necessary additional measurements of Reynolds stress tensor components were taken in the four corresponding midplanes, namely $x/D = 11.25, 13.75, 16.25, 18.75$, as well.

Vorticity Distribution

Within the x -range mentioned above the only significant vorticity component and, therefore, the only one considered here, is the streamwise x -component aligned with the crossflow direction which can be directly inferred from the measured projections of the velocity vectors in the planes $x = \text{Const.}$ Velocity gradients are computed using the three-point centred scheme. The vorticity distributions are illustrated for $x/D = 15$ in figure 2(a, b) for both arrangements showing the measured half of the “resulting” CVP. The term “resulting” should indicate that the TJICF flow phenomenon represents just an interaction of single JICFs and

that the dominant vortical structure formed downstream is a result of a certain merging process (in the *long-time-averaged* sense) of “more simple” vortical formations associated with the single JICF. This aspect is addressed in more detail separately in section Vortex Formation.

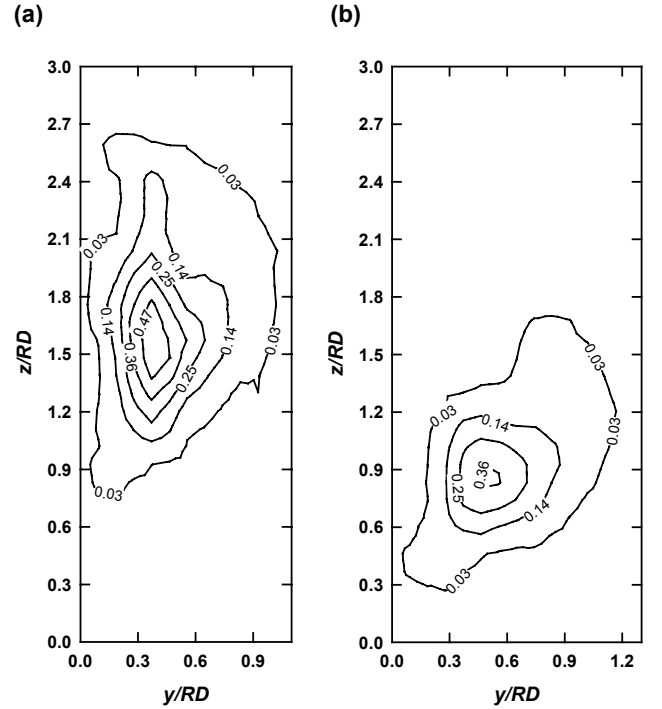


Figure 2. Negative vorticity for $x/D = 15$ ($x/RD = 1.875$): (a) tandem, (b) side-by-side arrangement (symbols as in (a)).

The coordinate RD -scaling, adopted in figure 2(a, b), has been found by Smith and Mungal [16] as the most appropriate scaling for the physical dimensions of the JICF. All flow quantities are normalized by D and U_C .

The vorticity distributions indicate that the tandem interaction of single jets produces a vorticity distribution somewhat similar to that of a single jet CVP (cf. [10]): kidney shape distribution (of significantly larger areal extent) of similar peak vorticity values having a systematic upward z -shift of about $1.4D$ (i.e. $0.175RD$). The side-by-side interaction of single jets results in a less pronounced vorticity distribution of smaller (but naturally wider) areal extent with systematic z -location of peak vorticity values only of about 55% relative to that of tandem structures.

Vorticity Transport

As far as turbulent vorticity transport is concerned, by intuition, the most intensive transport takes place near the centreline region where the greatest mean-vorticity gradients occur (cf. figure 2a, b). However, in turbulent flows the vorticity transport is driven by the gradients of Reynolds stress tensor components and anisotropy and inhomogeneity of Reynolds stresses play a crucial role. The centreline vorticity exchange between the single vortices of the CVP is a basic vorticity transport feature of the CVP vortical configuration [10]. Turbulent vorticity transport can be characterized and visualized in a straightforward manner by turbulent vorticity fluxes as defined in [8]. By introducing the antisymmetric turbulent vorticity flux-density tensor \mathbf{J} , the mean vorticity transport equation reads

$$\frac{\hat{D}\langle \boldsymbol{\omega} \rangle}{\hat{D}t} - \langle \boldsymbol{\omega} \rangle \cdot \text{grad}\langle \mathbf{u} \rangle + \langle \boldsymbol{\omega} \rangle \text{div}\langle \mathbf{u} \rangle = \nabla \cdot \mathbf{J} \quad (1)$$

where $\hat{D}/\hat{D}t \equiv \partial/\partial t + \langle \mathbf{u} \rangle \cdot \nabla$, $\nabla \cdot \mathbf{J} \equiv J_{ji,j} = -J_{ij,j}$. The tensor components J_{ij} are expressed purely in terms of gradients of the Reynolds stress tensor components as [8]

$$J_{ij} \equiv \langle u'_j \omega'_i \rangle - \langle u'_i \omega'_j \rangle = \epsilon_{ijk} T_{lk,l} \quad (2)$$

where, in the present 3D notation, the subscript comma precedes spatial partial derivatives, $T_{lk} \equiv \langle u'_l u'_k \rangle - \langle u'_m u'_m \rangle / 2 \delta_{lk}$, ϵ_{ijk} is the permutation symbol, δ_{lk} is the Kronecker delta symbol.

According to the coordinate system introduced (figure 1a, b), along the centreline there is only one generally non-zero component of the turbulent vorticity flux vector associated with the x -component of vorticity (for simplicity denoted as $\langle \omega \rangle$ below), namely the y -component. The y -component of the so-called *effective* (that is having generally a non-zero effect upon $\hat{D}\langle \omega \rangle / \hat{D}t$, see [8]) turbulent vorticity flux-density vector reads

$$J^y = (\langle w'^2 \rangle - \langle v'^2 \rangle)_z / 2 + \langle v'w' \rangle_y + \langle u'w' \rangle_x \quad (3)$$

(the subscripts stand for partial derivatives, the superscript y denotes the vector component).

The first flux term on the RHS of (3) dealing with normal Reynolds stresses does not contribute to the circulation decay, as will be discussed in the next section, and may be neglected. Hence, the only decisive flux terms are the second and third ones in (3). The reduced J^y flux distribution is determined from the turbulence statistics at four mid-planes with respect to five cross-sections of the measured velocity vector plots.

Figure 3(a, b) shows reduced J^y flux distributions for the four midplanes, namely for $x/D = 11.25, 13.75, 16.25$ and 18.75 ($x/RD = 1.41, 1.72, 2.03$ and 2.34). The tandem flux distributions indicate that while their first maxima at lower z -position roughly correspond—as to the z -position—to peak vorticity and upwash ($\langle w \rangle$ -component) velocity values, the second fastly decaying maxima correspond to the characteristic (i.e. for all x/D) upward “finger-like” vorticity lobe. An interesting flux minimum with negative values can be found in between these maxima. This flux minimum is caused by the extreme negative values of the last flux term in (3), $\langle u'w' \rangle_x$, associated with the 3D nature of the mean flow similarly as for the single JICF. Analogously, the second, fastly decaying, maxima are caused by the fastly decaying peak values of $\langle u'w' \rangle_x$, i.e. by the fastly decaying 3D effect. A quite different situation is given by the side-by-side case where the dominant flux minimum has to do with the significant region of negative values of $\langle v'w' \rangle_y$. An explanation for this “counter-gradient” transport with respect to mean vorticity distribution is given in section Vortex Formation.

Circulation Decay

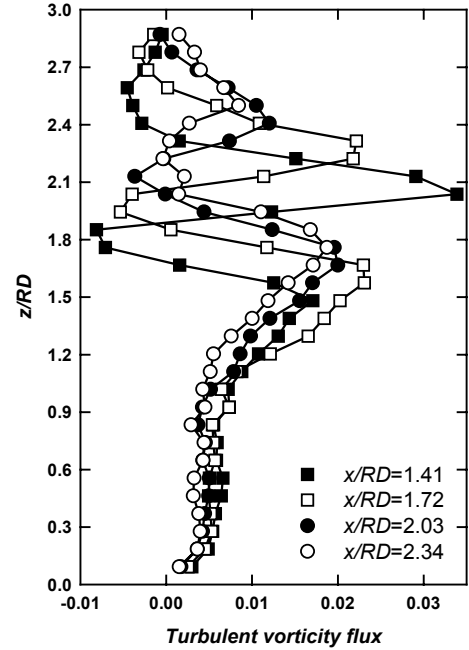
The circulation decay rate $d\Gamma/dt$ is described in terms of fluxes by

$$\frac{d\Gamma}{dt} = - \int_A (J_y^y + J_z^z) dA = \oint_C (J^y dz - J^z dy) \quad (4)$$

where C is a vortex boundary, $\Gamma = \int_A \langle \omega \rangle dA$. This expression

can be derived analogously as for planar case [9] where the kinematics of surface integrals are applied to the vorticity vector.

(a)



(b)

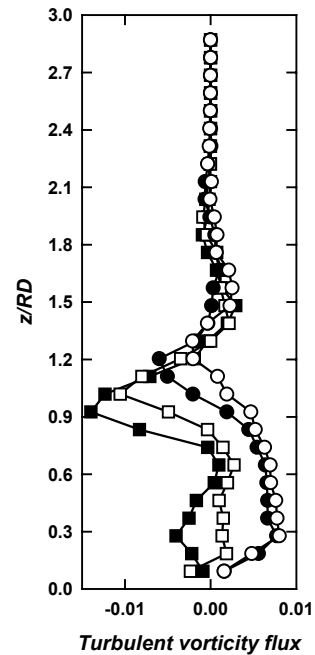


Figure 3. Turbulent vorticity flux: (a) tandem, (b) side-by-side arrangement (symbols as in (a)).

The key formula [17] (written below in the time-averaged sense)

$$\frac{d}{dt} \int_A \langle \mathbf{f} \rangle \cdot \mathbf{n} dA = \int_A \left(\frac{\hat{D}\langle \mathbf{f} \rangle}{\hat{D}t} - \langle \mathbf{f} \rangle \cdot \text{grad}\langle \mathbf{u} \rangle + \langle \mathbf{f} \rangle \text{div}\langle \mathbf{u} \rangle \right) \cdot \mathbf{n} dA \quad (5)$$

is employed and substituted from the vorticity transport equation in divergence form (1).

The circulation decay rate due to turbulent vorticity transport depends merely upon the turbulence properties (of anisotropy and inhomogeneity of Reynolds stresses) at the vortex contour, a significant part of which is just the centreline “separating” the single vortices of the CVP. The estimates of $d\Gamma/dt$ due to centreline turbulent vorticity transport are derived simply by

integration of $J^y dz$ over the relevant centreline interval I (for simplicity, the whole centreline velocity measurement interval is used for calculation)

$$\left(\frac{d\Gamma}{dt}\right)_{\text{centreline vorticity transport}} = \int_I J^y dz = \int_I (\langle v'w' \rangle_y + \langle u'w' \rangle_x) dz \quad (6)$$

where J^y is given by (3), reduced *a priori* in the first term. This reduction is possible provided that the integration limits are placed in the low turbulence regions outside the CVP. It should be recalled that the total circulation decay rate is given by (4).

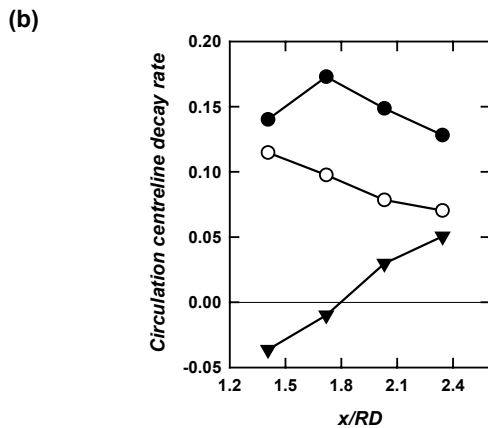
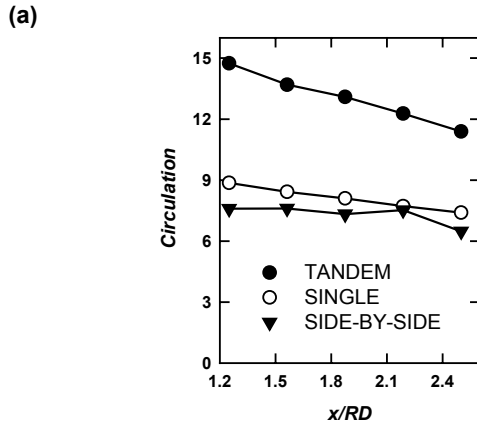


Figure 4. (a) Circulation. (b) Circulation centreline decay rate estimated by integration of turbulent vorticity fluxes (symbols as in (a)).

Figure 4(a, b) shows both the downstream development of the circulation and the values of $d\Gamma/dt$ due to centreline turbulent vorticity transport. For simplicity, the whole velocity measurement region was used for calculating Γ as a surface quadrature of $\langle \omega \rangle$. Both graphs of figure 4(a, b) indicate the same gross qualitative features regarding the circulation decay. While the tandem TJICF and single JICF systematically decay, the side-by-side arrangement exhibits for $10 \leq x/D \leq 17.5$ ($1.25 \leq x/RD \leq 2.19$) almost constant behaviour.

Vortex Formation

The obtained experimental data are in accordance with the expectations that the tandem arrangement CVP is a result of merging process of the stronger (initial) CVP of an upstream jet (figure 5a) with the slightly weaker CVP of a downstream “shielded” jet, the latter being with higher transverse penetration ability and having a certain lifting effect. The side-by-side arrangement CVP is expected to form during the strong interaction of inner vortices (figure 5b) rapidly cancelling each

other out. This short event of the vortex formation process may give the appearance of “counter-gradient” transport with respect to the mean vorticity distribution as indicated in figure 3(b).

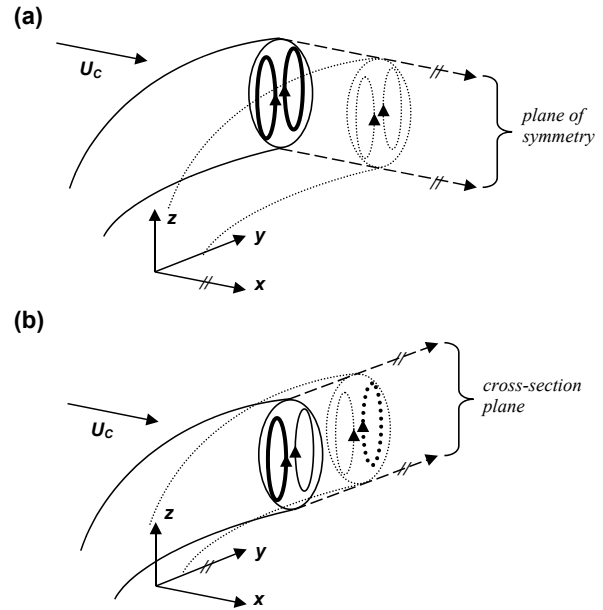


Figure 5. Vortex formation: (a) tandem, (b) side-by-side arrangement.

Conclusions

The dominant vortical structure and associated turbulent vorticity transport of tandem and side-by-side TJICF arrangements are experimentally examined, discussed and compared with the single JICF. Turbulent vorticity transport and circulation decay is described in terms of turbulent vorticity fluxes. The gross qualitative features of vortex formation process of the TJICF flow phenomenon—interaction of two single JICFs—are indicated.

Acknowledgments

V. Kolář gratefully acknowledges the support of the Royal Soc. (UK), Japan Soc. Promotion Sci., together with the support of GA Acad. Sci. of the Czech Rep. through grant A2060803 and of Acad. Sci. of the Czech Rep. through K2076106.

References

- [1] Barata, J.M.M., Durão, D.F.G., Heitor, M.V. & McGuirk, J.J., *AIAA J.* **29**, 1991, 595-602.
- [2] Cutler, A.D. & Bradshaw, P., *Exps. Fluids* **12**, 1991, 17-22.
- [3] Fric, T.F. & Roshko, A., *J. Fluid. Mech.* **279**, 1994, 1-48.
- [4] Gregoric, M., Davis, L.R. & Bushnell, D.J., *J. Heat Transfer* **104**, 1982, 236-240.
- [5] Holdemann, J.D. & Walker, R.E., *AIAA J.* **15**, 1977, 243-249.
- [6] Isaac, K.M. & Jakubowski, A.K., *AIAA J.* **23**, 1985, 1679-1683.
- [7] Karagozian, A.R., Nguyen, T.T. & Kim, C.N., *J. Propulsion* **2**, 1986, 354-360.
- [8] Kolář, V., Lyn, D.A. & Rodi, W., *J. Fluid Mech.* **346**, 1997, 201-237.
- [9] Kolář, V., *Proc. 13th Australas. Fluid Mech. Conf.* (eds. M.C. Thompson, K. Hourigan), Melbourne, Australia, 1998, 721-725.
- [10] Kolář, V., Savory, E. & Toy, N., *AIAA J.* **38**, 2000, 1763-1765.
- [11] Makihita, T. & Miyai, Y., *J. Fluids Engng.* **101**, 1979, 217-223.
- [12] Margason, R.J., *Proc. NATO AGARD Conf.*, CP-534, Winchester, UK, 1993, 1.1-1.41.
- [13] Morton, B.R. & Ibbetson, A., *Exp. Thermal Fluid Sci.* **12**, 1996, 112-133.
- [14] Papaspyros, J.N.E., Kastrinakis, E.G. & Nychas, S.G., *Appl. Sci. Res.* **57**, 1997, 291-307.
- [15] Savory, E. & Toy, N., *J. Fluids Engng.* **113**, 1991, 68-72.
- [16] Smith, S.H. & Mungal, M.G., *J. Fluid Mech.* **357**, 1998, 83-122.
- [17] Truesdell, C. & Toupin, R.A., *The Classical Field Theories. Encyclopedia of Physics* (ed. S. Flügge), Vol. III/1, 1960, p. 346.